Approaching the electromagnetic mechanism of surface-enhanced Raman scattering: from self-assembled arrays to individual gold nanoparticles

Lianming Tong,† Tao Zhu and Zhongfan Liu*

Received 10th February 2010
DOI: 10.1039/c001054p

Surface-enhanced Raman scattering (SERS) has been intensively explored both in theory and applications and has been widely used in chemistry, physics and biology for decades. A variety of SERS substrates have been developed in order to investigate the mechanisms behind, which give rise to the enormous enhancement even enabling single molecule detection. The Raman enhancement, which involves an electromagnetic enhancement (EM) and a chemical enhancement (CM), reflects both the physical principle of light/metal interactions and the molecule/metal interactions. In this *tutorial review*, we focus on the EM enhancement of SERS active substrates made of colloidal gold nanoparticles (GNPs), varying from self-assembled arrays down to single particles, for the purpose of investigating the EM coupling effect and probing the distribution of the induced electric field of single GNPs.

Introduction

Since its discovery in the 1970s, surface-enhanced Raman scattering (SERS) has exhibited its attraction in physics, chemistry and biology.[1–6] The related research field covers not only the enhancement mechanism of SERS but also its applications as a highly sensitive surface analytical tool for chemo/bio sensing.[4,6] There are two mechanisms: the electromagnetic (EM) enhancement induced by surface plasmon resonance (SPR) and the chemical enhancement (CM) originated from the charge transfer between the adsorbates and the substrate. The former, EM enhancement, typically requires a nanostructured metal substrate where the collective oscillation of the conduction electrons is confined, resulting in the so-called localized surface plasmon resonance (LSPR) under irradiation of light within a certain wavelength range.[7] The peak position and intensity of LSPR strongly depend on the material, roughness and surrounding medium of the nanostructures.[8,9] Nobel metals, such as gold and silver, are popular materials for SERS-active substrates because the resonance of their localized surface plasmon falls into the visible optical range where most of the commonly-used lasers are. The intensity of the induced electric field by the excitation of

Center for Nanochemistry, Beijing National Laboratory for Molecular Sciences, State Key Laboratory for Structural Chemistry of Unstable and Stable Species, College of Chemistry and Molecular Engineering, Peking University, Beijing 100871, P. R. China.
E-mail: zfliu@pku.edu.cn
† Current address: Department of Applied Physics, Chalmers University of Technology, 41296, Göteborg, Sweden.

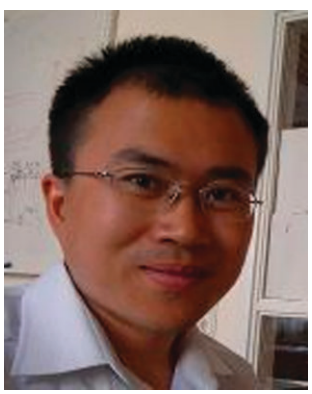

Lianming Tong

Dr Lianming Tong obtained his PhD in Physical Chemistry from the College of Chemistry and Molecular Engineering, Peking University, China, in 2007. His work was focused on controlled nanostructures of gold nanoparticles for surface-enhanced Raman scattering using self-assembly technique and atomic force microscope (AFM) manipulation. He is currently a postdoctoral fellow in the Department of Applied Physics, Chalmers University of Technology, Sweden, working on optical forces of metal nanostructures.

Tao Zhu

Dr Tao Zhu received his BSc Degree in Chemistry in 1987 and his PhD Degree in Analytical Chemistry in 1993 at Peking University, China. He joined Prof. Zhongfan Liu's group first as a post-doctoral fellow in 1993, and then became a faculty member in 1995 as associate professor. During 2001 and 2002, he visited Max-Planck Institute of Polymer Research in Mainz, Germany, working on the synthesis of functionalized metal clusters in Prof. Dr Wolfgang Knoll's group. Currently, he is a full professor at College of Chemistry and Molecular Engineering, Peking University, and his research interests lie in the size and shape controlled synthesis of metal nanoparticles, as well as the study of surface-enhanced Raman scattering characteristics in molecular and/or nanoparticles assemblies. He has published over 70 papers in refereed scientific journals.

LSPR can be approximated as $E \approx (\varepsilon(\omega) - \varepsilon_0)/(\varepsilon(\omega) + 2\varepsilon_0)\cdot E_0$, where $\varepsilon(\omega)$ is the frequency-dependent dielectric constant of the metal nanoparticles, ε_0 is the dielectric constant of the surrounding medium, and E_0 is the incident electric field. It can be seen that E is much stronger than E_0 when the denominator $(\varepsilon(\omega)+2\varepsilon_0) \rightarrow 0$, which means in resonance. Under such a resonant condition, therefore, the Raman probe molecules experience an enhanced incident field and emit Raman scattered photons, which are again enhanced by the localized electric field. In total, the EM enhancement of Raman scattering is proportional to the product of the incident field enhancement and emission enhancement, *i.e.*, $\left|\frac{E(\omega_0)}{E_0(\omega_0)}\right|^2 \cdot \left|\frac{E(\omega_{\mathrm{Raman}})}{E_0(\omega_{\mathrm{Raman}})}\right|^2$, where E and E_0 are the induced and incident electric field, and ω_0 and ω_{Raman} are the incident and Raman scattered frequency, respectively.[4] The EM enhancement is typically of $\sim 10^5$ or higher and dominates the overall enhancement. The chemical enhancement functions as an electronic resonance process, where the charge transfer occurs between the LUMO/HOMO of molecules and Fermi level of the metal substrate, which enhances the effective polarizability of the molecules.[10–12] This not only enhances the intensity of Raman scattering, typically by $1 \sim 2$ order-of-magnitude, but also changes the peak positions.

In order to investigate how EM enhancement depends on the size, shape and material of the SERS active substrates, and to excite LSPR efficiently for chemo/bio sensing, much efforts have been made in fabricating metal nanostructures for SERS in controlled manners.[13–16] The earlier techniques include electrochemically roughened electrodes, slat-driven aggregates in metal colloids and vacuum deposited metal films.[3,17] These are still important methods to study SERS, for example, to expand SERS substrates to transition metals.[18] Thanks to the rapid development of nanofabrication techniques, numerous new methods have been developed in fabricating controlled SERS active substrates, such as electron beam lithography (EBL), focused ion beam (FIB) and nano-sphere lithography (NSL), producing ideal templates with well-defined patterns for the study of both the EM coupling effect and the EM enhancement at single metal nanoparticle level.[13,19,20]

Due to the low cost and the ease of synthesis/surface modification, colloidal metal nanoparticles have shown their popularity for SERS. In 1995, Freeman *et al.*[14] reported the strategy of making SERS-active substrate based on self-assembled gold colloids on a chemically modified glass surface through electrostatic interaction. The surface density of the particles on substrates and the interparticle distances are easily adjusted by changing the assembly time, in turn, tuning the EM coupling. On the other hand, chemical synthesis of nanoparticles of different size, shape and/or compositions (for example, core/shell nanoparticles) has also been extensively studied.[21,22]

This tutorial review will discuss SERS-active substrates developed from assembled gold nanoparticles (GNPs) arrays to individual GNPs structures manipulated by atomic force microscope (AFM) for the study of EM enhancement. From the assembled GNPs arrays, an average EM enhancement (from single particles and/or interparticle coupling) can be investigated. In order to exclude the averaging effect and perform a deeper investigation to the contribution from "hotspots", one has to scale it down to single particle level. For single particle SERS, a special Raman probe molecule, single-walled carbon nanotube (SWNT), can be used to probe the electric field distribution of single GNPs.

Raman probe molecules and SERS enhancement factors

Raman probe molecules should be chosen depending upon the surface property of the SERS substrate and its application. For example, colloidal metal nanoparticles are usually negatively charged, so Raman active probes with positive charges in aqueous can be used utilizing the electrostatic attraction. For gold substrates, aromatic thiol molecules are one of the most popular probes due to the strong Au–S bonding and the large scattering cross section of the benzene ring. Single-walled carbon nanotubes (SWNTs), due to its unique shape and Raman characteristics, have also been studied as Raman probles in SERS.[23–25] Last but not least, to choose a probe with or without resonant Raman effect, which differs in the resulted total enhancement, is crucial, especially for single molecule SERS and enhancement factor (EF) estimation.

The conventional EF value is calculated by dividing the *average* intensity of surface-enhanced Raman scattering of a single molecule by that of normal Raman scattering. However, this definition assumes an ideally uniform enhancement over the whole substrate, which is not the case in reality. Le Ru *et al.*[26,27] introduced a series of EF definitions depending on SERS applications, and demonstrated that single molecule SERS can be detected with an EF of $\sim 10^7$ instead of $\sim 10^{14}$ as earlier reported. Ref. 27 is strongly recommended for further reading in the context of EF, as well as single molecule SERS.

Zhongfan Liu

Dr Zhongfan Liu received his PhD from the University of Tokyo in 1990. After a post-doctoral fellowship at Institute for Molecular Science (IMS), Japan, he became an associate professor (1993), full professor (1993) and Cheung Kong Chair professor (1999) of Peking University. He is now the director of Institute of Physical Chemistry and the director of Center for Nano-scale Science and Technology of Peking University. He also serves as the President of Chinese Electrochemical Society and the chief scientist of the national basic research program for nanotechnology "Quasi-1D Semiconducting Nanomaterials". His research is devoted to developing nano/molecular electronic devices using carbon nanotubes, graphenes, nanoparticles and other unique nanomaterials together with the exploration of fundamental phenomena in nanoscale systems such as resonant and surface-enhanced Raman scatterings. Dr Liu has published over 300 peer reviewed journal articles.

In this tutorial review, we will discuss the Raman enhancement of SERS substrates varying from self-assembled arrays to single GNPs. Two issues should be addressed before we proceed. Firstly, since we evaluate the average enhancement of the whole substrate, we will use the conventional EF definition (except for the SWNTs case), the so-called SERS substrate EF, estimated as

$$EF = (I_{SERS}/I_{bulk})/(N_{bulk}/N_{surf}) \quad (1)$$

where I_{SERS} and I_{bulk} represent the measured intensities of a selected band from a SERS spectrum and a normal Raman spectrum of a bulk sample, respectively, and N_{surf} and N_{bulk} represent the number of molecules which contribute to the measured intensities in SERS and normal Raman spectra, respectively. Secondly, although we will mainly focus on the EM enhancement, the CM enhancement, however, typically contributes $\sim 10^1$–10^2 to the overall SERS enhancement and is not ignorable. It is difficult to separate the CM contribution from that of EM if the molecules are in contact with the metal substrates. In the case where they are not in physical contact, CM can be reasonably excluded. A recent report by Uetsuki *et al.* gave a good demonstration.[28] In general, in order to obtain a reliable comparison of the EM enhancement (typically larger than 10^5), Raman probes with similar molecular structures should be used. More detailed discussion on the CM enhancement can be found elsewhere.[11,12]

EM Enhancement of self-assembled GNP arrays

The disadvantage of SERS-active substrates made of electrochemically roughened electrodes and aggregated colloids is that the roughness of the substrates is difficult to control. Since the EM enhancement is extremely sensitive to the surface roughness, one single nanoscale protrusion or crevice may dominate the SERS enhancement from the whole detected area.[29,30] Hence, it is important to make SERS substrates of uniform and homogeneous nanostructure arrays for EM enhancement investigation. There are several important techniques along this line, such as self-assembly of metal nanoparticles,[14,31] electron beam lithography (EBL)[20] and nanosphere lithography (NSL).[15] Among these methods, we will address the approach of self-assembled colloidal GNPs in this tutorial review. In a chemically synthesized gold colloid, the particle size is typically well monodispersed and easily controlled by changing the ratio of the reductant and the oxidant.[22] What is more, the average interparticle distance on a substrate can be adjusted simply by varying the assembling time and particles concentration in the colloid, making it a controllable substrate to investigate the EM enhancement of SERS.

Interparticle EM coupling

When the interparticle distance between two particles is close enough, the induced electric fields of single particles overlap with each other and give rise to the total field. This is particularly pronounced if the polarization of the incident light is parallel to the dimer axis.[32,33] The critical gap distance between two metal nanoparticles, below which the EM coupling occurs, is approximately the diameter of a single particle. Within the EM coupling range, excited by a parallel incident electric vector, the resonance of localized surface plasmon of a dimer redshifts with respect to that of single particles, and an enhancement of several orders of magnitude in the near-field intensity was found.[32,34] In a perpendicular configuration, the LSPR peak exhibits a slight blue-shift due to the cancellation of the induced dipoles, and only a small field enhancement results. On self-assembled arrays, where nanoparticles are randomly distributed, the incident electric vector always has a component parallel to adjacent particles. Hence, a field enhancement, and consequently the Raman enhancement, is expected.

Colloidal GNPs (negatively charged) can be assembled on aminopropyltriethoxylsilane (APTMS) modified silicon surfaces (positively charged) to form arrays.[35] By adjusting the assembling time, surface densities of GNPs can be tuned on different arrays, where the average interparticle distances can be found from statistical results over several areas on a sample. Probe molecules, aromatic thiols, are then chemically adsorbed on the particles by immersing the samples with GNP

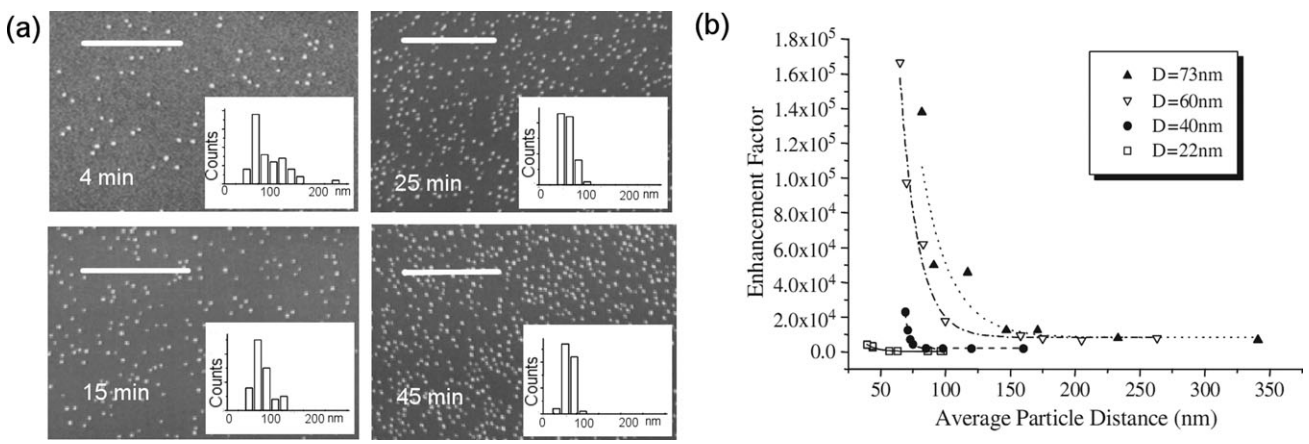

Fig. 1 (a) SEM images of self-assembled ~22 nm GNPs arrays after immersion time of 4, 15, 25 and 45 min, respectively. Scale bar: 1 μm. Insets show the corresponding statistical interparticle distances. (b) EF values of self-assembled GNPs arrays as a function of average interparticle distances. Adapted from ref. 35.

arrays in a thiol/ethanol solution. Fig. 1(a) shows an example of ~22 nm GNP arrays after an assembling time of 4, 15 25 and 45 min, respectively. The nearest neighbor distance histograms are shown as the insets.

As shown in Fig. 1(b), the Raman enhancement keeps constant at large interparticle distances, indicating that the interparticle EM coupling does not occur and the EF is basically that of single particles, which is $\sim 4.0 \times 10^2$ under 633 nm laser excitation. The average EF values of larger single GNPs, ~40 nm, ~60 nm, and ~73 nm, are found as $\sim 1.9 \times 10^3$, $\sim 7.5 \times 10^3$, and $\sim 1.1 \times 10^4$, respectively. However, one should note that in such GNPs arrays, there are unavoidably a small portion of aggregates, which are possibly from in the colloid or formed during the self-assembly process. Such aggregates usually give a much higher enhancement than the average value, thus have to be ruled out for EF estimation by taking the average of SERS spectra of similar intensities on randomly selected spots on the substrates and excluding those with extremely high intensities.

At higher surface coverage, that is, with decreasing interparticle distance, the EF increases remarkably due to the EM coupling effect. The critical center-to-center distances, below which a sharp increase of enhancement is found, are ~50, ~80, ~120 and ~150 nm for the ~22, ~40, ~60 and ~73 nm GNPs, respectively, approximately twice diameters of the particles, namely, one diameter in gap distance. Since the GNPs in a colloid are negatively charged due to the adsorption of citrate ions, the electrostatic repulsive force between the adjacent particles limits the nearest gap distances between the GNPs during self-assembly. For such arrays, the nearest gap distances for ~22, ~40, ~60 and ~73 nm GNPs are ~8, ~10, ~10 and ~7 nm, giving corresponding maximum EF values of $\sim 1.0 \times 10^3$, $\sim 2.3 \times 10^4$, $\sim 1.4 \times 10^5$ and $\sim 1.7 \times 10^5$, respectively.

Close-packed GNP arrays

With respect to the above-mentioned self-assembled arrays, an onward issue is how much Raman enhancement is expected if the interparticle distance decreases more until nanoparticles are close to or even in physical contact. To this end, efforts have been made by several groups.[36,37] Wei *et al.*[36] used a specially designed molecule, thiolated calixarene, to encapsulate GNPs (16–170 nm), forming self-organized 2-dimensional (2D) hexagonal close-packed (hcp) arrays. Using the same thiolated calixarene as Raman probe, they found a Raman enhancement of 10^4–10^7 on such arrays (see Fig. 2). Another approach is to utilize the capillary force during a solvent evaporation process, where surfactant encapsulated nanoparticles are driven to form 2D hcp arrays. Wang *et al.*[37] reported 2D hcp arrays fabricated using this method with cetyltrimethylammonium bromide (CTAB) functionalized GNPs (~50 nm in diameter), from which an empirical Raman enhancement of $\sim 10^8$ was found for p-mercaptoaniline (pMA), a nonresonant molecule, under 785 nm laser excitation. Using GNPs dispersed in ethanol and an immersed glass slide at a 30° inclination, Hossain *et al.*[38] obtained relatively smaller 2D hcp arrays of 50 nm GNPs with an average center-to-center distance of 54.5 nm, and an EF of 10^6–10^7 was reported for CV molecules using 647 nm excitation.

We have also previously shown 2D hcp GNPs arrays fabricated by solvent evaporation driven self-organization of thiolated alkane functionalized GNPs.[39] Although alkyl-thiol molecule has been used as Raman probes in SERS,[40] their Raman cross section is considerably lower than those commonly used probes, such as aromatic thiols and dye molecules. We thus chose 4-*tert*-butylbenzylmercaptan (4-tBBM) molecules, which facilitates the fabrication of 2D hcp arrays and has a relatively large Raman cross section.[41] Fig. 3(a) shows typical SEM images of the close packed arrays with GNPs of ~22 nm, ~65 nm and ~78 nm respectively. Under 633 nm laser excitation, the corresponding EF values are $\sim 4.7 \times 10^5$, $\sim 1.9 \times 10^7$ and $\sim 1.1 \times 10^7$, respectively. The representative surface enhanced Raman scattering spectra measured on different close-packed GNPs arrays are shown in Fig. 3(b), with the corresponding EF values shown in Fig. 3(c).

The highest EF is $\sim 1.9 \times 10^7$, found on ~65 nm GNPs array. It is two orders of magnitude higher than the highest EF obtained from self-assembly arrays of ~60 nm GNPs ($\sim 1.7 \times 10^5$). The nearest interparticle distance for the close-packed GNPs array is about twice the molecule length (~1 nm) and that of the self-assembled arrays is ~10 nm. Obviously, the extra enhancement is originated from the much stronger near-field coupling at near-contact gap distance. It is worth noting here that, in all SERS spectra measured on the above substrates in Fig. 3, there is always the CM contribution to the total enhancement. Since it is usually of $\sim 10^1$–10^2 (much lower than EM enhancement), and the probes are of the similar molecular structures for the substrates, it is reasonable to compare the EF values between the self-assembled arrays and the closed packed arrays. However, if one compares the EF values between different works, one should always keep in mind the difference in the excitation wavelengths and the probe molecules, in particular, resonant or nonresonant types. For reference purposes, the theoretical calculation of EM enhancement of Raman scattering on 2D close-packed arrays with different diameter/gap distance ratios can be found in ref. 42, where the EM enhancement of 5×10^8 was demonstrated.[42]

From self-assembled arrays to individual GNPs

To achieve a high EM enhancement, the incident laser wavelength has to be close to the resonance peak of the LSPR, which is determined by many parameters: the size, shape, material of the nanoparticles and interparticle distances.[8,9] On self-assembled GNP arrays, as mentioned above, it is an averaged enhancement that is obtained. The arrays unavoidably contain particles with size/shape variation and non-identical interparticle distances, which is crucial at very close separations (a few nanometers). It is of fundamental interest to understand the enhancement and near-field distribution at single particle level. The first single-molecule SERS was discovered on single Ag nanoparticles and/or aggregates of a few nanoparticles, where a Raman enhancement of $\sim 10^{14}$ was reported for single molecules located at so-called "hotspots".[29,43] One has to note that, single molecule SERS

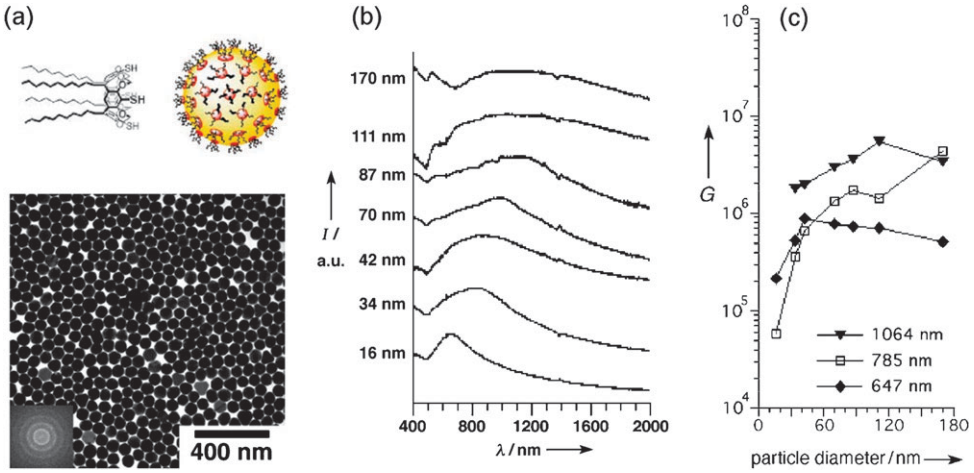

Fig. 2 (a) Molecular structure of thiolated calixarene and TEM image of a 2D hcp array. (b) Extinction spectra of different 2D hcp arrays of GNPs. (c) EF values as a function of particle sizes under different laser excitation. Adapted from ref. 36.

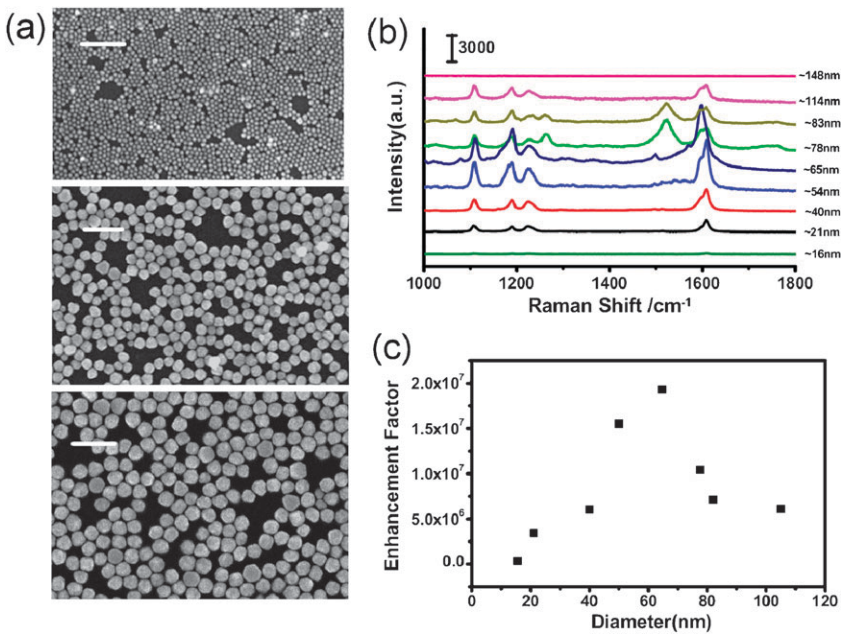

Fig. 3 (a) SEM images of 2D close-packed arrays of ~22, ~65 and ~78 nm GNPs, respectively. Scale bar: 200 nm. (b) Representative SERS spectra of 4-tBBM molecules on 2D closed-packed GNPs arrays under 633 nm laser excitation. (c) Size dependence of the EF values.

has been widely explored using different strategies, such as Langmuir–Blodgett, tip-enhanced Raman and bi-analyte techniques, and a much lower EF value (~10^7) has been found efficient enough to detect single molecules.[27,44]

Recent studies have demonstrated more details of SERS on single nanoparticles and small clusters, for example, the polarization dependence of dimers and trimers,[45,46] the near-field distribution around different shapes of nanoparticles,[47] SERS on well-defined nanoparticle clusters fabricated using EBL assisted self-assembly,[48] and SERS on dimers/trimers of well controlled Au@Ag core/shell structures.[49] The single-particles-SERS studies performed based on colloidal nanoparticles, however, usually pick up aggregates from a colloid with certain salt concentrations. From a controllability point of view, the precise manipulation of individual nanoparticles for SERS is still lacking. It has been reported that atomic force microscope (AFM) can be used to oxidise substrates in nanoscale regions and manipulate single nanoparticles.[50–52] Using AFM manipulation of nanoparticles for SERS, one sees the potential of investigating SERS on the *same* particles with well-adjusted interparticle distances and alignments.

SERS on controlled alignment of GNPs by AFM manipulation

Controlled nanostructures of one, two, three and four GNPs, respectively, can be fabricated using AFM manipulation,[53] as shown in Fig. 4 and 5. 4-Methylbenzenethiol (4-MT) was used as Raman probe molecules for SERS measurements. In Fig. 4(a), GNPs of 54 nm, 60 nm, 50 nm and 62 nm in

diameter were moved from other areas to form a linear alignment but were separated beyond the EM coupling distances. The enhancement is thus the sum of the contribution from individual particles and shows no polarization dependence (solid squares in Fig. 4(d)) since the particles are spherical. The EF from single particles (of approximately 60 nm in diameter) under 633 nm laser excitation is obtained as $\sim 6.0 \times 10^4$. However, when the particles are moved within near-field coupling distance, the Raman enhancement exhibits a dramatic increase and strong polarization dependence, which is shown in Fig. 4(b) and (c). The EF increases to $\sim 2.2 \times 10^7$ and $\sim 9.0 \times 10^5$ under parallel and perpendicular polarization, respectively. The EF values for near-contact alignment of two and three particles of similar size (62 nm, 60 nm and 64 nm, respectively) are also obtained and plotted in Fig. 5.

The EF values for these GNP structures under perpendicular polarization are of the same order of magnitude as for single particles because of the weak coupling between adjacent particles. However, under parallel polarization, the EFs increase from $\sim 6.0 \times 10^4$ for single particles to $\sim 1.9 \times 10^6$, $\sim 1.0 \times 10^7$ and $\sim 2.2 \times 10^7$, respectively. The relative (normalized to that without EM coupling) enhancement for near-contact alignments of two and three GNPs and for four coupled GNPs is 16, 56 and 92 for parallel polarization, and 1.7, 3.0 and 3.8 for perpendicular polarization, respectively. These results indicate two facts. One is that a strong EM coupling occurs when the laser polarization is parallel to the alignment and becomes stronger with more GNPs. While the polarization is perpendicular, there is a weak EM coupling, which increases slightly with the number of GNPs. On the other hand, from the logarithm plot in Fig. 5 (dashed lines), one can expect that the enhancement would saturate at certain number of GNPs excited by 633 nm laser.

It is worth noting here that the exact gap distances are not distinguishable by AFM imaging due to the well-known convolution effect of the AFM tips. From the estimation of peak-to-peak distance in AFM cross section analysis, the nearest gap distances for the alignments with two and three GNPs are estimated to be $\sim$1–2 nm. Because the EM coupling strongly depends on the interparticle distance, the nearest distances of one or two nanometres difference may result in a considerable change in the EM enhancement. Moreover, the nearest gap distances of the four GNP alignments are $\sim$25 nm, $\sim$45 nm and $\sim$25 nm, respectively, which are relatively large. At closer separations, the EM enhancement is expected to be stronger.

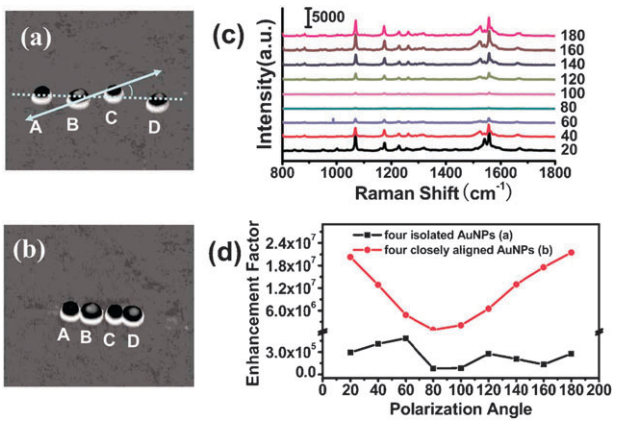

Fig. 4 AFM images and Raman enhancement of four GNPs manipulated by AFM. (a) and (b) AFM images (800 × 800 nm) of four GNPs beyond and within EM coupling range. (c) SERS spectra from the structure in (b) at different polarization angles. (d) Polarization dependence of the EF for the two structures in (a) and (b). Adapted from ref. 53.

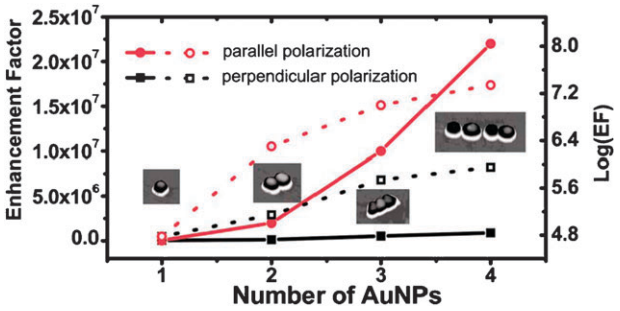

Fig. 5 EFs of one, two, three and four GNPs alignment. Solid lines represent a linear plot (left *y*-axis) and dashed lines represent a logarithm plot (right *y*-axis). Adapted from ref. 53.

Single GNP enhanced Raman scattering of SWNTs

The above results of Raman enhancement on controlled structures with a few nanoparticles exclude the average effect of GNPs to a great extent compared to the nanoparticle self-assembly arrays. However, it is still an averaged effect in terms of molecules. Since the localized electric field distribution is inhomogeneous around the surface of nanostructures, the molecules at different sites experience different EM enhancement, which is averaged out during the estimation of enhancement factors. It is notoriously difficult to solve this problem in experiments because the precise positions of the probe molecules, which are normally small organic molecules, on the particle surfaces are unknown.

Single-walled carbon nanotube (SWNT), due to its unique intrinsic Raman characteristics and one-dimensional geometry, is a special candidate for SERS.[23] Individual SWNTs can even be used to probe the near-field distribution of a metal tip or single GNPs.[24,25] Compared to SERS of bulk SWNTs with GNP aggregates or on roughened gold films,[23] there are two advantages in single-GNP enhanced SWNTs SERS. One is that the separation between a SWNT and a GNP can be well distinguished from cross section analysis of an AFM image. In the case where the SWNT is *not* in physical contact with the particles, the overall Raman enhancement is only from pure EM enhancement since there is no pathway for CM. On the other hand, the separation can be easily adjusted by pushing the GNP using AFM manipulation. These, in total, make it an ideal system for the investigation of pure EM enhancement. By changing the incident polarization and the distance between the SWNTs and GNPs, the intensity distribution of the localized electric field of single GNPs can also be probed by the SWNTs.

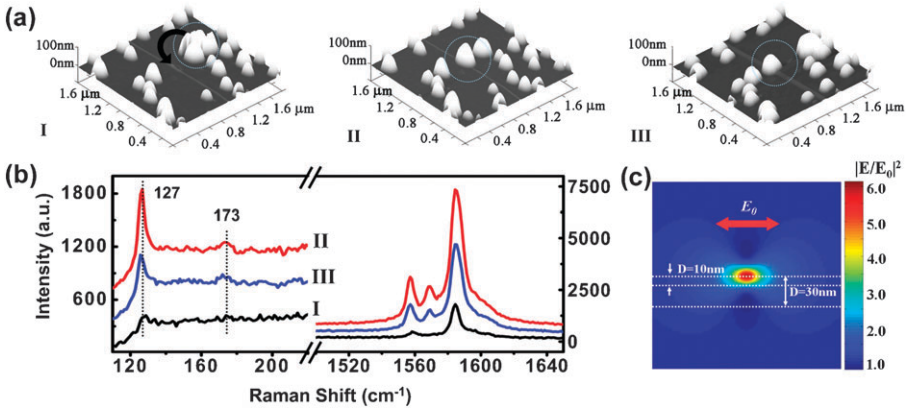

Fig. 6 (a) AFM images of a SWNT and GNPs before and after AFM manipulation. (b) Corresponding Raman spectra of the SWNT enhanced by a single GNP at different separations. (c) Theoretical calculation of the induced electric field on the substrate where the GNP sits. Adapted from ref. 25.

By placing a GNP beside a SWNT *via* AFM manipulation (Fig. 6(a)), the Raman scattering intensity can be dramatically enhanced, as shown in Fig. 6. After a precise adjustment of the distance between a GNP and an individual SWNT using AFM manipulation, the distance dependence of Raman enhancement is further investigated. As shown in Fig. 6(b), the Raman scattering intensity increases ~3 and ~6 times when the distance decreases to ~30 nm and ~10 nm, respectively, compared to that at ~200 nm separation where there is no enhancement. This is in accordance with our extended Mie-theory calculations, which show a stronger electric field at closer separation (Fig. 6(c)).

A more detailed investigation was performed to study the polarization and distance dependence of Raman enhancement of a SWNT. The results are shown in Fig. 7, where a GNP of 78 nm in diameter is manipulated to enhance the Raman scattering of a SWNT. Two effects should be taken into account in the analysis of the polarization dependence: the polarization dependence of resonant Raman scattering of the SWNT itself and that of the local electric field around the GNP experienced by the SWNT.[32,54] These two effects have an opposite polarization dependence and the overall Raman scattering intensity is determined by the net result. The experimental results in Fig. 7(a) show that the Raman scattering intensity is the maximum at parallel polarization and minimum at perpendicular polarization, indicating that the polarization dependence of SWNT itself, *i.e.*, the selection rule of Raman excitation, plays a major role. At all polarization angles, the Raman scattering intensity becomes higher with decreasing separation distance.

It should be noted that at 90 degrees polarization angle, the Raman scattering intensity is near-zero without enhancement from the GNP. Once enhanced by a GNP, the SWNT exhibits detectable signals. The relative enhancement in this case is infinite. Hence, for a reasonable comparison, we define a different EF by normalizing the Raman intensities to that at parallel polarization without enhancement I_{x0}, $M(\theta) = I_\theta/I_{x0}$, where θ is the polarization angle. As shown in Fig. 7(b), the Raman enhancement is in well agreement with our theoretical simulations based on a modest modification of the conventional EM enhancement calculations. Since only the parallel

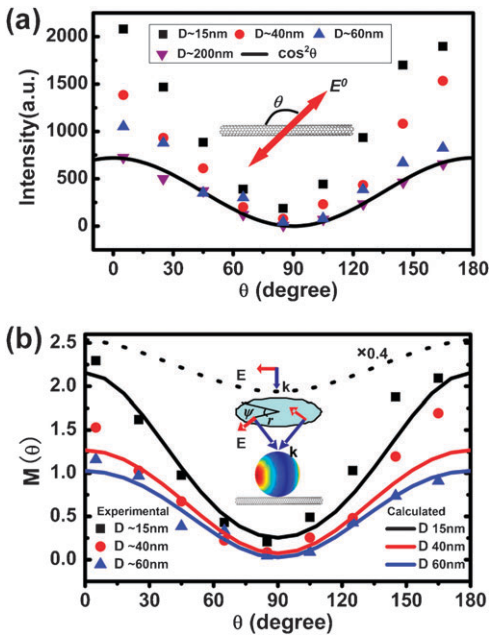

Fig. 7 (a) Raman scattering intensities of a SWNT at different separations to a 78 nm GNP. The inset shows the definition of the polarization angle. (b) Raman enhancement calculated from (a) and corresponding theoretical simulation. See text for details. Adapted from ref. 25.

electric component excites the Raman scattering of a SWNT, one should only consider the parallel component of the induced electric field instead of the total field. The dashed line in Fig. 7(b) shows the calculated Raman enhancement from the total electric field. It is obviously overestimated compared to the experimental results. This modification, in principle, holds for SERS of all the one-dimensional molecules with polarization dependent Raman scattering characteristic.

From Fig. 7, one can extract the distance dependence of the enhancement at different polarization angles. Because the intensity of the induced electric field decays as $1/r^3$ in the near-field range and Raman enhancement scales approximately with $|E/E_0|^4$, taking a scaling factor r^2 of the shell of molecules at distance r into account, one obtains the theoretical distance

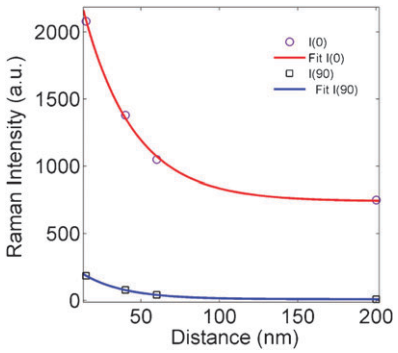

Fig. 8 Distance dependence of Raman scattering intensity of a SWNT enhanced by a 78 nm GNP under parallel polarization (open circles) and perpendicular polarization (open squares), respectively, and corresponding exponential fit (solid lines).

dependent Raman intensity $I \propto (1+r/a)^{-10}$ from the pure EM enhancement, where a is the radius of the particle.[55] Fig. 8 shows the plots of Raman intensities of the G band at $\sim$1580 cm^{-1} (the tangential mode of sp^2 hybridized carbon–carbon vibration) as a function of separation between the particle and the SWNT under parallel and perpendicular polarizations, respectively. In both cases, the fitting of $(1+r/a)^{-10}$ did not apply. In our experiments, at least three factors could cause deviation to the theoretical model. Firstly, although we assume the GNP is ideally spherical, the small features of roughness on the surface are unknown. Secondly, the Raman scattering of the SWNT under consideration itself involves a resonant process.[54] Thirdly, the $(1+r/a)^{-10}$ dependence holds for molecules at different r normal to the surface, *i.e.*, at the same azimuthal angle, which is not the case here.

However, an exponential fit, $I = I_0 + A\cdot\exp(-d/l)$, agrees well with the experimental data with R-square greater than 0.98 as shown in Fig. 8. The open circles and squares represent data extracted from Fig. 7(a) and the solid lines are corresponding exponential fits. The parameter l here can be defined as decay length. For both parallel and perpendicular polarization, a decay length of $\sim$22 nm was obtained. In the study of tip-enhanced Raman scattering of individual SWNTs, Hartschuh *et al.*[24] found that the decay length for a silver tip with 10–15 nm radius is $\sim$11 nm. This value could depend on the size, shape and material of the particle/tip, as well as the surrounding medium, and is worthwhile to be further investigated in different systems with pure EM enhancement.

Summary

The route of studying SERS on substrates from self-assembly arrays of GNPs to individual GNP structures manipulated by AFM is introduced. Qualitative results of the EM enhancement can be obtained on the self-assembled arrays, showing a sharp increase of Raman enhancement with decreasing average interparticle distances within near-field coupling range. On 2D hcp GNP arrays, a much higher enhancement can be found compared to the self-assembled GNPs arrays due to the much closer separation and thus the much stronger coupling effect. To rule out the averaging effect over particles of different size, shape, and interparticle distances, one has to focus on single particle SERS. The strategy of using AFM manipulation to fabricate controlled nanostructures of GNPs for SERS is discussed. Furthermore, using individual SWNTs as Raman probe molecules, it is possible to probe the near-field distribution of a single GNP.

Recent reports on the distribution of "hotspots"[56] and the application of SERS for highly sensitive sensing[57] imply that, after the decades since its discovery, SERS is still of fundamental and practical interest to the wide community of physics, chemistry and biology. The investigation of the SERS mechanism not only helps one to further understand its physical/chemical nature but also enables reliable designs for the application of SERS as a highly sensitive analytical tool. On this basis, the development of ideal SERS active substrates is of great importance and of practical applications for chemo/bio sensing.

Acknowledgements

The research was supported by the National Natural Science Foundation of China (Grants 50821061, 20833001, 20973013) and the Ministry of Science and Technology of China (Grants 2007CB936203, 2006CB932403).

References

1 M. Fleischmann, P. J. Hendra and A. J. McQuillan, *Chem. Phys. Lett.*, 1974, **26**, 163–166.
2 M. G. Albrecht and J. A. Creighton, *J. Am. Chem. Soc.*, 1977, **99**, 5215.
3 J. A. Creighton, *Surf. Sci.*, 1983, **124**, 209–219.
4 G. C. Schatz, M. A. Young and R. P. VanDuyne, *Top. Appl. Phys.*, 2006, **103**, 19–46.
5 A. Campion and P. Kambhampati, *Chem. Soc. Rev.*, 1998, **27**, 241–250.
6 M. Moskovits, *Rev. Mod. Phys.*, 1985, **57**, 783.
7 H. Wang, D. W. Brandl, P. Nordlander and N. J. Halas, *Acc. Chem. Res.*, 2007, **40**, 53–62.
8 K. L. Kelly, E. Coronado, L. Zhao and G. C. Schatz, *J. Phys. Chem. B*, 2003, **107**, 668–677.
9 K. S. Lee and M. A. El-Sayed, *J. Phys. Chem. B*, 2006, **110**, 19220–19225.
10 M. Osawa, N. Matsuda, K. Yoshii and I. Uchida, *J. Phys. Chem.*, 1994, **98**, 12702.
11 A. Otto, *J. Raman Spectrosc.*, 2005, **36**, 497–509.
12 B. N. J. Persson, K. Zhao and Z. Zhang, *Phys. Rev. Lett.*, 2006, **96**, 207401.
13 M. J. Banholzer, J. E. Millstone, L. Qin and C. A. Mirkin, *Chem. Soc. Rev.*, 2008, **37**, 885–897.
14 R. G. Freeman, K. C. Grabar, K. J. Allison, R. M. Bright, J. A. Davis, A. P. Guthrie, M. B. Hommer, M. A. Jackson, P. C. Smith, D. G. Walter and M. J. Natan, *Science*, 1995, **267**, 1629–1632.
15 A. J. Haes, C. L. Haynes, A. D. McFarland, G. C. Schatz, R. R. Van Duyne and S. Zou, *MRS Bull.*, 2005, **30**, 368–375.
16 P. J. G. Goulet and R. F. Aroca, *Anal. Chem.*, 2007, **79**, 2728–2734.
17 M. Kahl, E. Voges, S. Kostrewa, C. Viets and W. Hill, *Sens. Actuators, B*, 1998, **51**, 285–291.
18 Z. Tian, B. Ren and D. Wu, *J. Phys. Chem. B*, 2002, **106**, 9463–9483.
19 T. R. Jensen, M. D. Malinsky, C. L. Haynes and R. P. Van Duyne, *J. Phys. Chem. B*, 2000, **104**, 10549–10556.
20 L. Gunnarsson, E. J. Bjerneld, H. Xu, S. Petronis, B. Kasemo and M. Käll, *Appl. Phys. Lett.*, 2001, **78**, 802–804.
21 C. B. Murray, C. R. Kagan and M. G. Bawendi, *Annu. Rev. Mater. Sci.*, 2000, **30**, 545–610.
22 Y. Xia, Y. Xiong, B. Lim and S. E. Skrabalak, *Angew. Chem. Int. Edit.*, 2009, **48**, 60–103.

23 K. Kneipp, H. Kneipp, P. Corio, S. D. M. Brown, K. Shafer, J. Motz, L. T. Perelman, E. B. Hanlon, A. Marucci, G. Dresselhaus and M. S. Dresselhaus, *Phys. Rev. Lett.*, 2000, **84**, 3470–3473.
24 A. Hartschuh, E. J. Sanchez, X. Xie and L. Novotny, *Phys. Rev. Lett.*, 2003, **90**, 095503.
25 L. Tong, Z. Li, T. Zhu, H. Xu and Z. Liu, *J. Phys. Chem. C*, 2008, **112**, 7119–7123.
26 E. C. Le Ru and P. G. Etchegoin, *J. Chem. Phys.*, 2009, **130**.
27 E. C. Le Ru, E. Blackie, M. Meyer and P. G. Etchegoin, *J. Phys. Chem. C*, 2007, **111**, 13794–13803.
28 K. Uetsuki, P. Verma, T. Yano, Y. Saito, T. Ichimura and S. Kawata, *J. Phys. Chem. C*, 2010, **114**, 7515–7520.
29 S. Nie and S. R. Emory, *Science*, 1997, **275**, 1102–1106.
30 H. Xu, E. J. Bjerneld, M. Käll and L. Borjesson, *Phys. Rev. Lett.*, 1999, **83**, 4357–4360.
31 A. Wei, B. Kim, B. Sadtler and S. L. Tripp, *ChemPhysChem*, 2001, **2**, 743.
32 H. Xu, J. Aizpurua, M. Käll and P. Apell, *Phys. Rev. E*, 2000, **62**, 4318–4324.
33 E. Prodan, C. Radloff, N. J. Halas and P. Nordlander, *Science*, 2003, **302**, 419–422.
34 L. Gunnarsson, T. Rindzevicius, J. Prikulis, B. Kasemo, M. Käll, S. Zou and G. C. Schatz, *J. Phys. Chem. B*, 2005, **109**, 1079–1087.
35 Z. Zhu, T. Zhu and Z. Liu, *Nanotechnology*, 2004, **15**, 357–364.
36 A. Wei, *Chem. Commun.*, 2006, 1581–1591.
37 H. Wang, C. S. Levin and N. J. Halas, *J. Am. Chem. Soc.*, 2005, **127**, 14992–14993.
38 M. K. Hossain, Y. Kitahama, V. Biju, T. Itoh, T. Kaneko and Y. Ozaki, *J. Phys. Chem. C*, 2009, **113**, 11689–11694.
39 S. Liu, T. Zhu, R. Hu and Z. Liu, *Phys. Chem. Chem. Phys.*, 2002, **4**, 6059–6062.
40 M. Rycenga, J. M. McLellan and Y. Xia, *Chem. Phys. Lett.*, 2008, **463**, 166–171.
41 L. Tong, T. Zhu and Z. Liu, *Sci. China Ser. B*, 2007, **50**, 520–525.
42 D. A. Genov, A. K. Sarychev, V. M. Shalaev and A. Wei, *Nano Lett.*, 2004, **4**, 153–158.
43 K. Kneipp, Y. Wang, H. Kneipp, L. T. Perelman and I. Itzkan, *Phys. Rev. Lett.*, 1997, **78**, 1667–1670.
44 N. P. W. Pieczonka and R. F. Aroca, *Chem. Soc. Rev.*, 2008, **37**, 946–954.
45 T. Shegai, Z. Li, T. Dadosh, Z. Zhang, H. Xu and G. Haran, *Proc. Natl. Acad. Sci. U. S. A.*, 2008, **105**, 16448–16453.
46 K. Imura, H. Okamoto, M. K. Hossain and M. Kitajima, *Nano Lett.*, 2006, **6**, 2173–2176.
47 M. Rycenga, P. H. C. Camargo, W. Li, C. H. Moran and Y. Xia, *J. Phys. Chem. Lett.*, 2010, **1**, 696–703.
48 B. Yan, A. Thubagere, W. R. Premasiri, L. D. Ziegler, L. Dal Negro and B. R. M. Reinhard, *ACS Nano*, 2009, **3**, 1190–1202.
49 G. Chen, Y. Wang, M. Yang, J. Xu, S. J. Goh, M. Pan and H. Chen, *J. Am. Chem. Soc.*, 2010, **132**, 3644–3645.
50 X. Ling, X. Zhu, J. Zhang, T. Zhu, M. Liu, L. Tong and Z. Liu, *J. Phys. Chem. B*, 2005, **109**, 2657–2665.
51 R. Resch, D. Lewis, S. Meltzer, N. Montoya, B. E. Koel, A. Madhukar, A. A. G. Requicha and P. Will, *Ultramicroscopy*, 2000, **82**, 135–139.
52 S. Kim, D. C. Ratchford and X. Li, *ACS Nano*, 2009, **3**, 2989–2994.
53 L. Tong, T. Zhu and Z. Liu, *Appl. Phys. Lett.*, 2008, **92**.
54 G. S. Duesberg, I. Loa, M. Burghard, K. Syassen and S. Roth, *Phys. Rev. Lett.*, 2000, **85**, 5436–5439.
55 B. J. Kennedy, S. Spaeth, M. Dickey and K. T. Carron, *J. Phys. Chem. B*, 1999, **103**, 3640–3646.
56 Y. Fang, N.-H. Seong and D. D. Dlott, *Science*, 2008, **321**, 388–392.
57 J. Li, Y. Huang, Y. Ding, Z. Yang, S. Li, X. Zhou, F. Fan, W. Zhang, Z. Zhou, D. Wu, B. Ren, Z. Wang and Z. Tian, *Nature*, 2010, **464**, 392–395.

